Study and test of the rebuncher for SARAF-LINAC phase II

Lu Zhao, Xiaowen Zhu, Jonathan Dumas, Didier Chirpaz, Tom Joannem, Francis Gohier, Nicolas Solenne, Patrice Guiho, Remy Braud, Olivier Piquet, et al.

Study and test of the rebuncher for SARAF-LINAC phase II

Lu Zhao[a,*], XiaoWen Zhu[a], Jonathan Dumas[a], Didier Chirpaz[a], Tom Joannem[a], Francis Gohier[a], Nicolas Solenne[a], Patrice Guiho[a], Remy Braud[a], Olivier Piquet[a], Guillaume Ferrand[a], Sébastien Ladegaillerie[a], Claude Marchand[a], Francoise Gougnaud[a], Romuald Duperrier[a], Didier Uriot[a], Leo Weissman[b], Boaz Kaizer[b,c], Eli Farber[c], Matthieu Michel[d], Jean-Francois Leyge[d]

[a] *IRFU, CEA, Université Paris-Saclay, F-91191 Gif-sur-Yvette, France*
[b] *SNRC, Israel*
[c] *Department of Electrical Engineering and Department of Physics, Ariel University, Ariel, Israel*
[d] *GANIL,IFRU, CEA, Université Paris-Saclay, Caen, France*

Abstract

In order to match the beam exiting the RFQ to the superconducting cavities and to minimize the longitudinal beam extension, three rebunchers will be installed in the Medium Energy Beam Transport (MEBT) of SARAF-LINAC phase II. CEA is in charge of the design and fabrication of the copper-plated stainless steel, 3-gap rebunchers. Beam dynamic simulation leads to the global MEBT design. The rebuncher was successfully conditioned to the RF power of 4.4 kW required for CW operation, with sufficient power margin. A solid state power amplifier of 10 kW developed by SNRC is used during the RF test. The rebuncher shows a good performance in terms of the dissipated power, peak temperatures and vacuum level.

Keywords: `RF power, Buncher, MEBT, Beam dynamic, Linac`

*Corresponding author:
Email address: `zhaolu.715@gmail.com` (Lu Zhao)

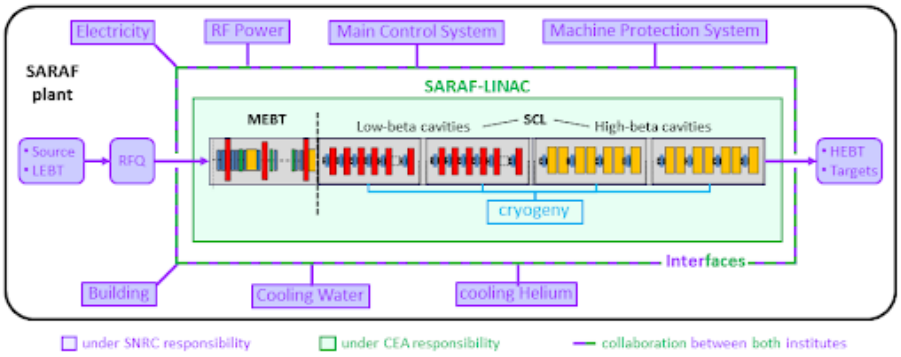

Figure 1: Schematic view of SARAF-LINAC:

1. Introduction

The upgrade of the Soreq Applied Research Accelerator Facility (SARAF), managed by the Soreq Nuclear Research Center (SNRC), aims to deliver 5 mA CW deuteron and proton beams at 40 and 35 MeV respectively [1]. The Commissariat à l'Energie Atomique et aux énergies alternatives (CEA) is in charge of the design and building of a Medium Energy Beam Transport (MEBT) line and the SuperConducting Linac (SCL) [2] to complete the existing structure of phase I [3] consisting of an ECR ion source, a Low Energy Beam Transport (LEBT, a Radio Frequency Quadrupole (RFQ) and an High Energy Beam Transport (HEBT) line. Figure 1 illustrates a schematic drawing of the SARAF-LINAC project. The SCL has been discussed in the previous article [4]. A 5-meter MEBT line (see Figure 2) consisting of three normal conducting rebunchers, eight quadrupoles, three H/V slit boxes, two diagnostics boxes and Structural-Vacuum-Cooling (SVC) sub-system, plays no acceleration goal but has other essential functionalities [5]:

1. to match the beam from the RFQ to the SCL,
2. to measure the beam current and the transverse and longitudinal beam distributions,
3. to steer the beam on the accelerator axis,

4. to clean the beam if necessary (elimination of halo) to stop the pulsed beam (low power) during the tuning process of the injector alone,
5. to cope with the high vacuum gradient between RFQ and downstream SC structure.

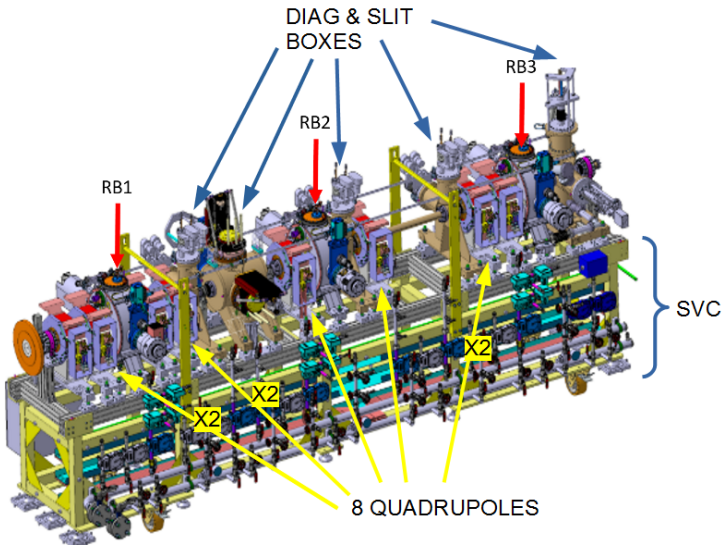

Figure 2: MEBT line 3D model.

We use the TraceWin code [6] to optimize the beam performances. The beam dynamic analysis defines the optimal position of different elements of the MEBT to manage the beam coming from RFQ and match it to the SCL. Three rebunchers are mandatory to avoid an excessive longitudinal extension of the beam which would cause unacceptable emittance growth and losses in SCL [7].

Different configurations of the bunching cavity, such as number of gaps, stem geometry, have been studied in order to minimize the total power consumption and the peak power density [8]. The IFMIF-type copper-plated stainless steel cavity was selected to operate at 176 MHz. Numerical simulation was performed to optimize the RF design and the thermal budget of rebuncher. The specification of the rebuncher were defined and given in Table 1. To compensate the mechanical manufacturing tolerances, the simulation error and the thermal

drift, a frequency tuning system is needed. A closed-loop control system drives the tuning system according to the measured phase between the injected and transmitted RF signals of the rebuncher.

Table 1: rebuncher requirements

Requirement	Value	Units
Frequency	176	MHz
Synchronous phase	-90	degree
Quality factor	> 6600	
Drift tube aperture	40	mm
Flange to flange distance	< 280	mm
Tuning range	> 600	kHz
Max. local temperature	100	°C

Additionally, some technical conceptions have to be considered. According to our experiences from SPIRAL2, the rebuncher has to be properly cleaned to present residual outgassing (lower than $3 \cdot 10^{-5} mbar \cdot l \cdot s^{-1}$) when operated in CW, at design voltage. It should be equipped with a pumping CF flange, leaving an open surface higher than $45 \cdot cm^2$ [9]. In order to ensure RF impedance continuity, multi-contacts have to be installed at each flange besides the vacuum metal sealed joint.

To validate the rebuncher design, the RF power test for each rebuncher is essential before installing in the MEBT line. Furthermore, the RF power test can clean the inner side of rebuncher to enhance its vacuum performance.

2. Beam dynamic of MEBT

Beam dynamic studies define the specifications for the rebunchers. In the regular operation mode of the SARAF machine, the MEBT adapts the beam from the RFQ to the SC-Linac and needs to include an optional chopper, not yet defined but deviates the beam to a beam dump with a voltage of 800V,

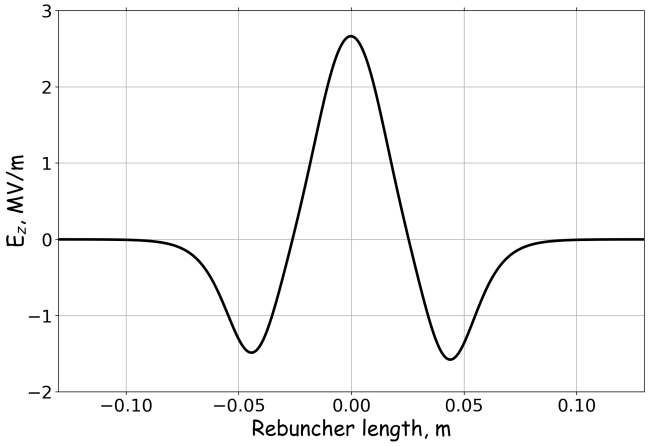

Figure 3: On-axis field rebuncher for E_0TL= 120 kV.

which makes the MEBT longer and calls for 3 rebunchers with max. E_0TL of 120kV (see on-axis field of the rebunchers in Figure 3).

The most demanding power for the rebunchers is set by the highest intensity beam of the heaviest species considered (D^+, 5mA). The Twiss parameters of this beam from the RFQ are shown in table 2.

Table 2: Twiss parameters for 5 mA deuton RFQ output

α_x	-0.56
α_y	0.06
α_z	-0.26
β_x	0.16 $mm/\pi.mrad$
β_y	0.20 $mm/\pi.mrad$
β_z	0.64 $mm/\pi.mrad$
Norm. RMS $\epsilon_{xx'}$	0.20 $\pi.mm.mrad$
Norm. RMS $\epsilon_{yy'}$	0.20 $\pi.mm.mrad$
Norm. RMS $\epsilon_{zz'}$	0.12 $\pi.MeV.deg$

The optics in the MEBT is such that the quadrupoles gradients are listed in

Table 3 and the rebunchers E_0TL in Table 4. The resulting MEBT configuration and beam envelope are illustrated in Figure 4. Envelope peaks are optimized in order to minimize the biggest peak, inducing by this way the balancing of quadrupole and rebuncher forces, therefore minimizing also the biggest forces [7].

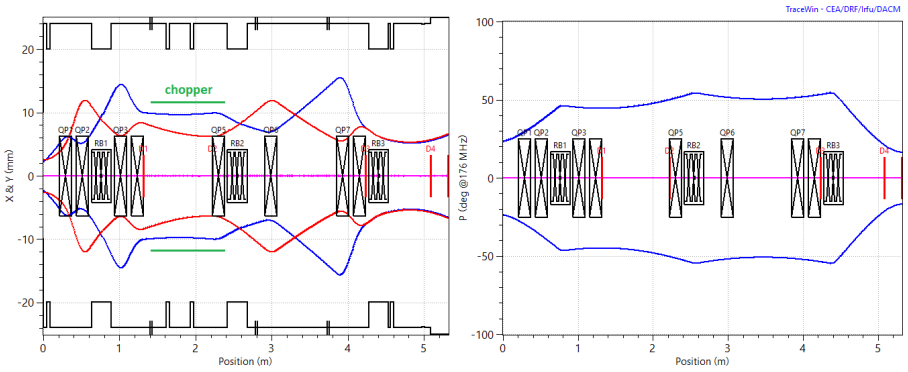

Figure 4: 3σ transverse (left), x in blue and y in red. and longitudinal (right) envelopes in the MEBT. [7]

The goal is to keep the beam footprint in the longitudinal phase space at the end of the MEBT within a 0.2 MeV and 50° range around the reference particle in order to match the SC-Linac acceptance, see Figure 5.

Table 3: Required gradient for the quadrupoles in a regular operation mode

	QP1	QP2	QP3	QP4	QP5	QP6	QP7	QP8
gradient (T/m)	9.4	-9.7	7.1	-4.3	1.7	-3.3	6.4	-6.1

Table 4: Required voltage for each rebuncher in a regular operation mode

	RB1	RB2	RB3
Voltage (kV)	74.7	32.3	90.7

During the commissioning of the machine, the longitudinal emittance of the beam coming from the RFQ needs to be evaluated. One of the proposed

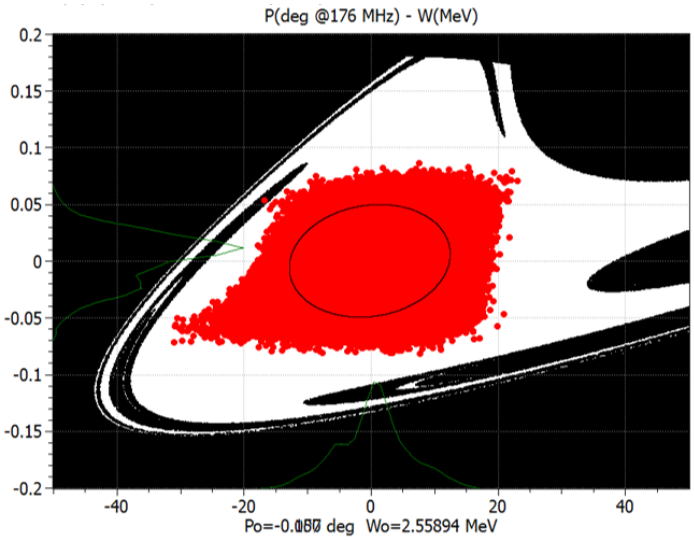

Figure 5: MEBT longitudinal distribution (in red), compared with the SC-linac acceptance (in white).

methods is to measure the bunch length evolution when varying the effective voltage in the first rebuncher [10]. In these conditions, an effective voltage up to 150 kV is necessary as shown in Figure 6, in order to reach a minimum in the bunch length and derive the Twiss parameters. Nevertheless, this measurement will be done only with pulsed beam and with pulsed RF in the rebuncher, (duty cycle (dc) $< 40\%$) to limit the rebuncher warming. A lower voltage would affect the precision of the beam longitudinal emittance evaluation leading to the degradation of the longitudinal beam matching to the SCL, such as emittance growth and higher beam loss rate.

3. RF study

The rebuncher design is based on the experience accumulated with the SPIRAL2 rebuncher [11]. Considering the total power consumption and the peak power density within the allocated length of 280 mm flange to flange, the IFMIF-type cavity, declined in 3-gap version, with 40 mm aperture, fits well our requirements. The basic structure of the 3-gap rebuncher has been given in our previous

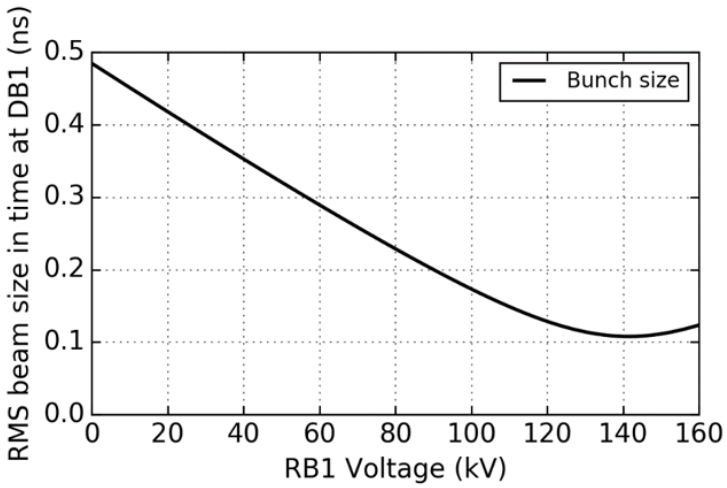

Figure 6: RMS beam bunch vs voltage in the first rebuncher.

published work [12]. Figure 7 gives a general view of SARAF2 rebuncher with the main components separated. Cu-plated stainless steel constitutes the outer tank. However, solid copper is used for the fabrication of quarter wave stems and the stem flanges, where most of the power is dissipated and where higher thermal conductivity is mandatory. Solid copper is also used for beam ports and drift tubes, which endure the high electric field as well. To keep the leakage rate better than several 10^{-8} mbar l/s , the double gaskets have been preferred for each flange connection: a vacuum Al joint with the GETELECT spira-shield commercial RF gaskets are used for the front flange. For other flange connections, the commercial CF copper gaskets (different sizes) are used with the same RF gaskets.

3.1. Tuner

Figure 8(a) shows the inner view of the rebuncher consisting of a fixed, a motorized tuners, two stems and a power coupler loop. Two tuner holders are welded on the tank bottom to limit the top flange deformation (in order to limit the frequency shift) under vacuum and to isolate higher order modes caused by the movable tuner.

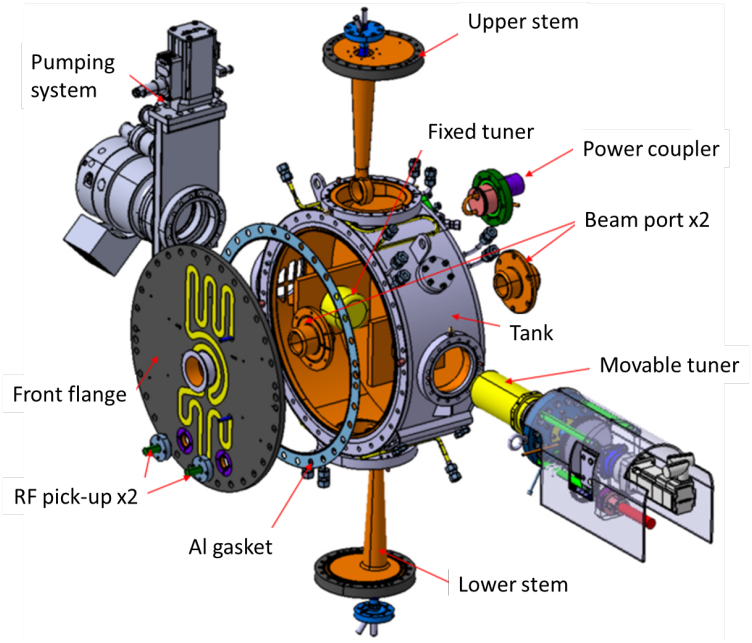

Figure 7: 3-gap rebuncher cavity components [12]

The height of cylinder (fixed tuner) has to be evaluated before copper plating process to have symmetrical field distribution around the stem rings. That is to say, the rebuncher should have the resonance frequency of 176 MHz under the required vacuum condition when the tuner distance (the distance between the movable tuner and the stem ring) equals to the fixed distance (the distance between the fixed tuner and the stem ring). The tuner can compensate the frequency deviation due to the mechanical deformation induced by power dissipation etc. The movable tuner swings slightly around the symmetrical position in the regular operation. Thus, the effect of non-symmetrical field can be neglected.

The movable tuner has a tuning range of 30 mm which corresponds to 1.5 MHz frequency tuning range as shown in Figure 8(b) (blue line). The measured frequency is higher than the simulated value (red line), because the frequency is measured under the atmospheric condition (1 bar), the frequency will decrease about 230 kHz due to the rebuncher deformation under the vacuum condition.

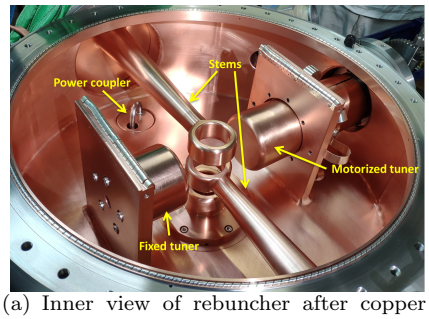

(a) Inner view of rebuncher after copper coated

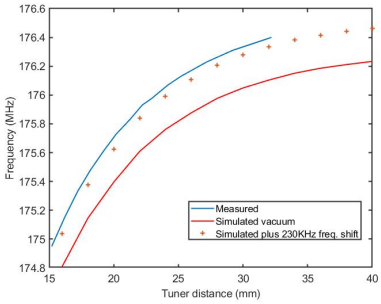

(b) Frequency turning range

Figure 8: Rebuncher with tuning system

Thus, considering this decrease in frequency (red plus plot), the simulated results show a good agreement to the measured values.

3.2. Frequency vs Temperature

Considering the initial cooling water temperature of $T_0 = 25°C$, the rebuncher body temperature with full power energy is about 55 ° (given in section 4). The temperature raise of 30°C will induce a series of variations of the rebuncher, such as, the thermal expansion and the deformation at some hot spots of rebuncher. These will cause a frequency drift about of 98 kHz for resonant frequency of 176 MHz.

When the generator frequency f is very close to the cavity resonance frequency f_0, the relation between the detuned phase angle ϕ and frequency detuning Δf is given by the equation [13]:

$$tan\phi \approx 2Q_L \frac{\Delta f}{f} \tag{1}$$

So that one degree variation of temperature can yield the frequency tuning about $\Delta f = 3$ kHz, corresponding a phase variation of 6.8° calculated by the equation 1.

4. Thermal study

The main cavity and flanges are in stainless steel with copper coating inside. This technology is less expensive than massive copper, less bulky and easier to weld. The difficulty is to cool properly stainless steel because of its low conductivity compared to copper (16 W/m/k against 400 W/m/K for copper). Every heated area has to be cooled locally. A series of multiphysics coupled RF and thermal-stress analyses have been performed to investigate the temperature map of rebuncher. The simulation was run with the code ANSYS. Thermal calculations have been performed with thermal load increased by two margin coefficients: 20% on total RF loss, which were calculated with a 30% margin on the surface conductivity. Then we expect our results to be overestimated. Moreover, they are obtained at design voltage (120 kV) and not at required voltage (105 kV)[14]. According to our experiences, we designed the cooling circuit (c1 to c5 and c8, c9) grooved in the material thickness of the cavity, while two copper pipe brazed out of the caviy wall for C6 and C7, as shown in Figure 9. Inside the cavity, the stems made of copper are cooled by conduction

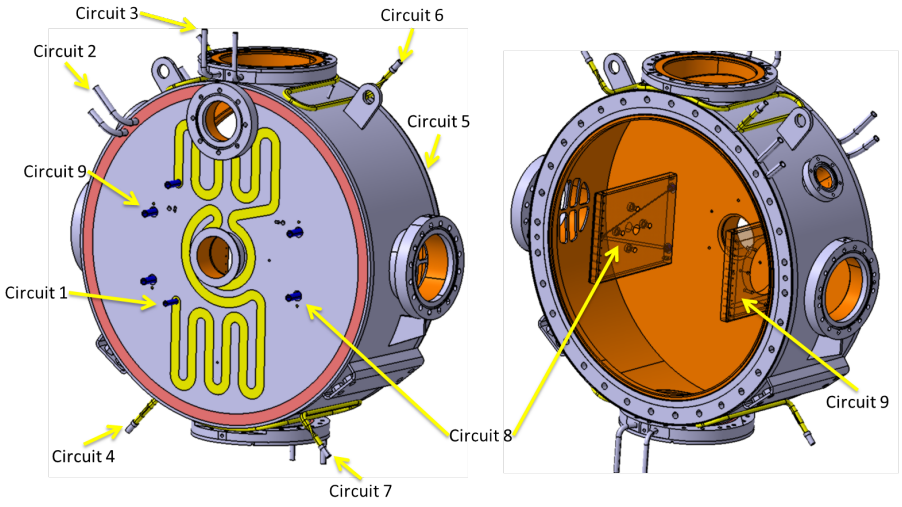

Figure 9: Cooling circuits of the cavity tank and zoom on the stem flange .

from the stem neck and the movable tuner is cooled by the copper pipe brazed

inside as shown in Figure 10.

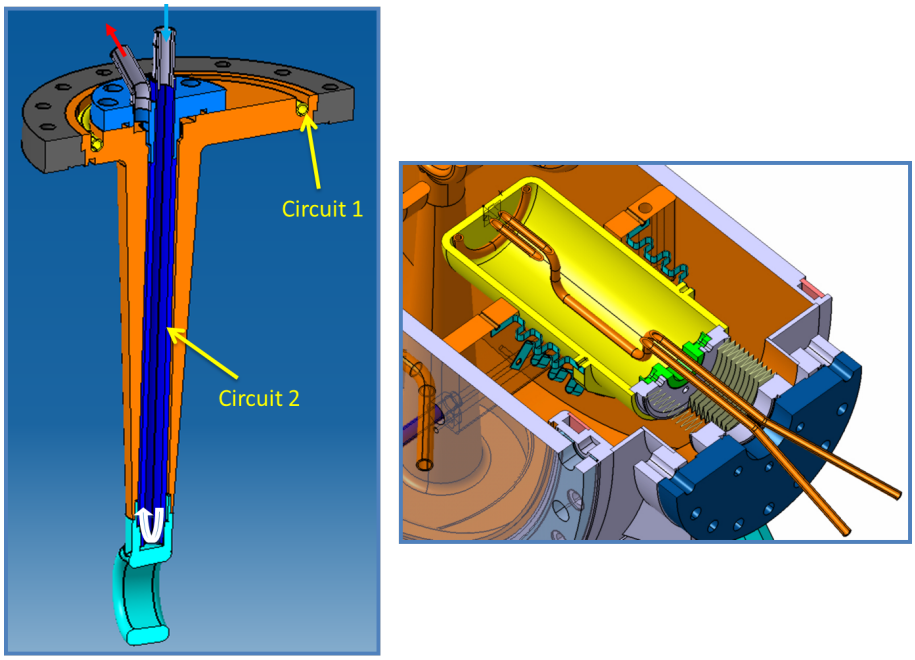

Figure 10: Inner cooling circuits.

With the designed cooling circuit, the stem neck should stay below 60 $°C$. On the rebuncher body, a small spot just under the beam port flange could have a max. temperature almost of 95 $°C$ if this area is not cooled, 53 $°C$ if it is cooled [9].

5. RF test

RF performances of the rebuncher were measured using a Vector Network Analyzer. The quality factor Q_0 of the rebuncher is about 7000 calculated by $Q_0 \approx 2 \times Q_L$ where Q_L is measured of 3500.

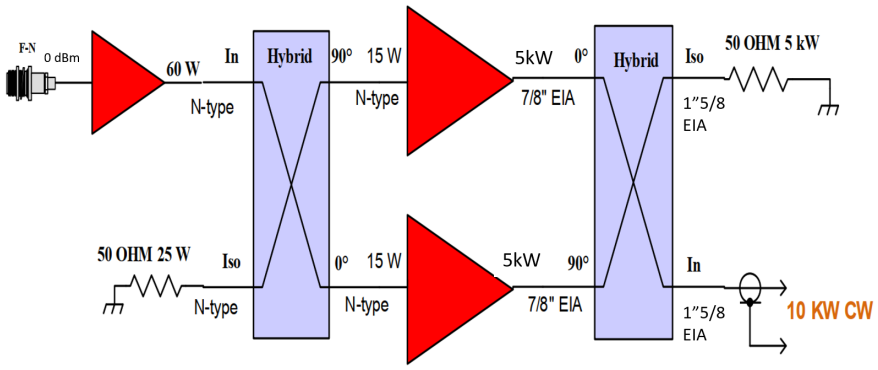

Figure 11: 10kW HPA conceptual diagram.

5.1. RF power amplifier

A compact narrow-band Solid State Power Amplifier(SSPA) capable of delivering 10 kW CW RF power at 176 MHz was developed at SNRC for SARAF-linac Phase II. The 10 kW amplifier is built by combining the RF power from two 5 kW amplifiers using 3 dB 90° High Power Quad Hybrid Couplers (HPQHC). The 5 kW amplifiers are combined from eight 800 W LDMOS water cooled amplifier modules equipped with an internal circulators and RF loads. The conceptual electrical diagram is presented in Figure 11. This RF amplifier is installed at the outside of the rebuncher RF test bunker. The amplifier was first tested by connecting the amplifier output to a water cooled 50 Ω load, and driven by an RF generator, it was tested up to maximum output power of 12kW. A 1'5/8 rigid coaxial line was used to conduct the RF power from the RF power amplifier to the rebuncher.

5.2. Acquisitions and Control system

Under the CEA EPICS environment (IEE framework[15]), a control system for the test bench (data acquisition, system configuration and automatic conditioning) is developed using EPICS 3.15[16]. The system runs on a IOxOS IFC1210 VME card, and performs the high speed acquisitions (RF measurements) through an IOxOS ADC3111 mezzanine card (8 channels ADC 16-bit

250 Mps). It performs as well the slow acquisitions and controls (analogue or binary) through remote I/O Beckhoff modules using Modbus protocol with an EK9000 coupler. Experiments measurements and controls are archived continuously using EPICS Archiver Appliance [17].

5.3. Closed-loop tuning control

In the closed-loop tuning control system, a Siemens 1500 PLC and a S110 speed variator is responsible for driving the movable tuner based on the measured phase between the injected and transmitted RF signal. Figure 12 gives the response of the phase detector of AD8302 which shows a good linear in the range from -50° to 50°. The control of motor is divided in two regions: regu-

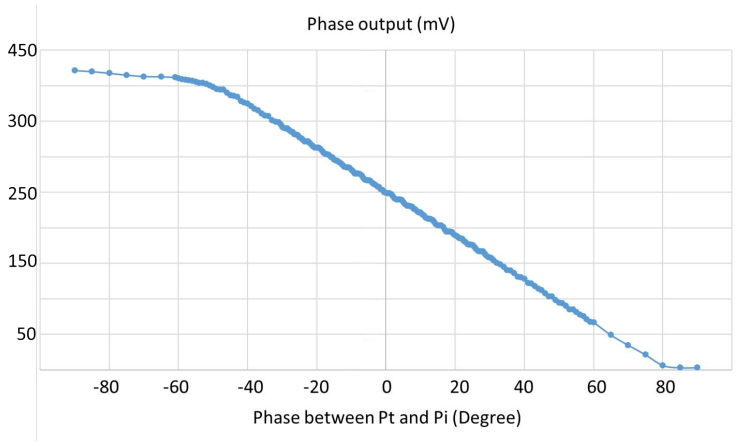

Figure 12: Output of phase detector.

lation and fast movement. For example, the phase between -20° to 20 ° (see figure 13) is the regulation area where the motor will move as a speed of 2 mm/s because of the relative low reflected power. Once the measured phase out of this area, the motor will bring the phase directly to 0° with a higher speed in order to avoid too much reflected energy. Note that, the closed-loop control will become disabled once the injected RF signal stops. During the RF power test, a slight phase variation was observed. Figure 14 illustrates the measured phase variation due to the cooling water temperature variation of $1°C$. The 0.037 V

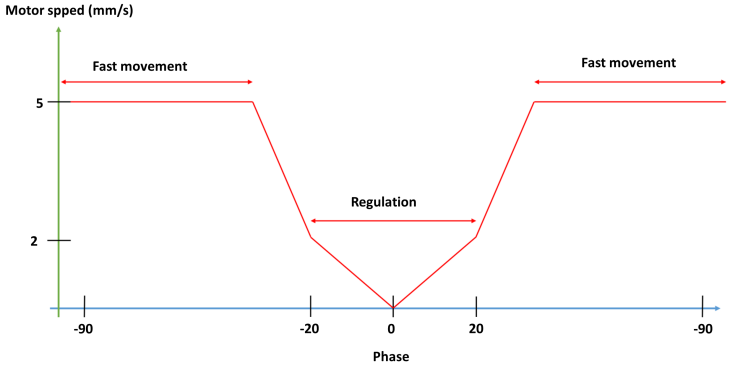

Figure 13: speed regulation for phase difference tuning

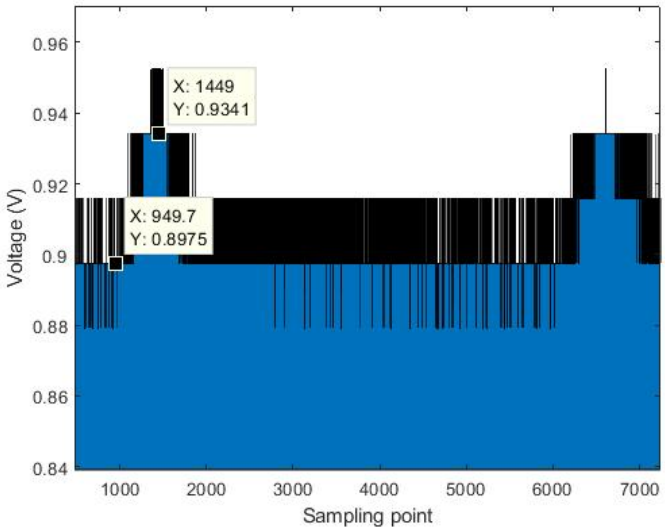

Figure 14: Phase variation as water temperature.

195 voltage variation corresponds à 7.32° of phase variation. This phase has a good agreement to the calculated value (6.8°) discussed in previous section §3.2. And this phase variation can be corrected by the closed-loop tuning system.

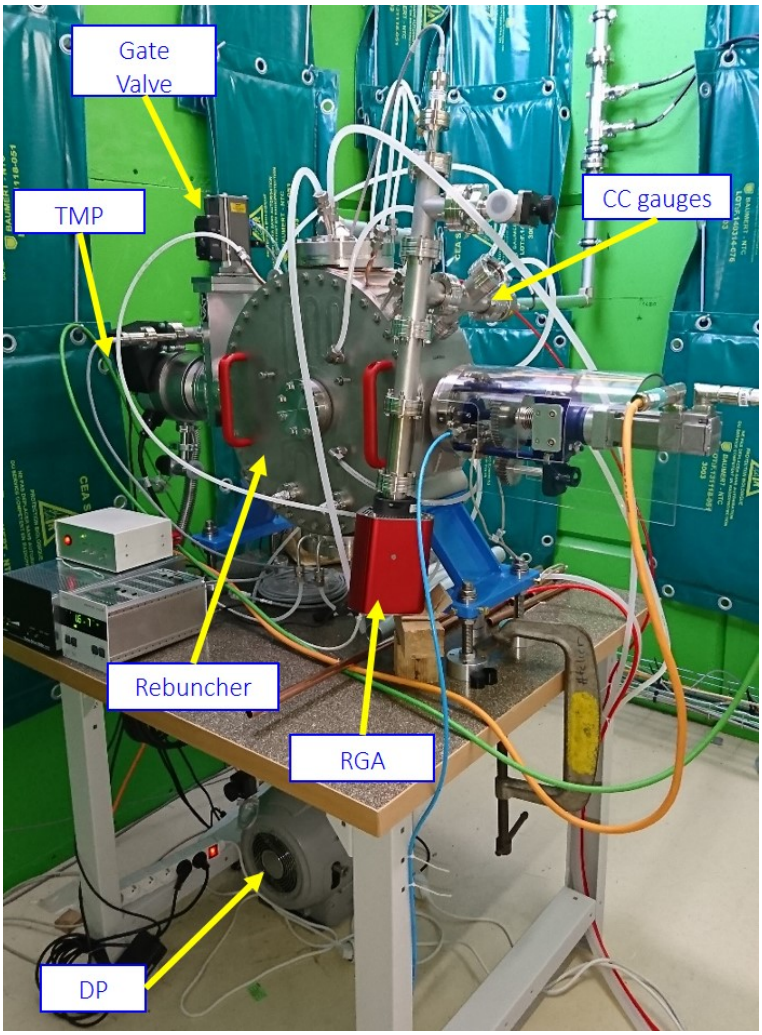

Figure 15: Full equipped rebuncher for RF power test.

5.4. RF Power Test

Figure 15 shows the rebuncher RF power test bench inside the bunker with the radiation shielding. The rebuncher has been successfully conditioned up to 4.4 kW in CW mode at a frequency of 176 MHz. The RF conditioning starts at a gentle condition, for example, a very low power level of 10 W and an RF pulse ratio of 1% with an RF pulse repetition of 1 Hz. With the control system, the power level and the pulse ratio increase automatically. The RF power will

decrease in case of a vacuum burst, ex. excessive reflections or sparking. Vacuum in the rebuncher is maintained to be better than 1×10^{-7} mbar during the RF conditioning. We observe that most multipacting occurs in the low energy region (from 200 to 550 Watt).

In addition, the gas composition in the rebuncher was changed by the RF conditioning as shown in table 5 and the vacuum quality was enhanced by a factor of three.

Table 5: Pressures and gas compositions in the rebuncher at three different moments (before/during/after RF conditioning).

	100h pumping	At the end of the RF conditioning	After conditioning
Pressure	$6.5 \cdot 10^{-8}$	$1.3 \cdot 10^{-7}$	$2.1 \cdot 10^{-8}$
H_2 (%)	20 %	75 %	30 %
H_2O (%)	80 %	25 %	70 %

6. Conclusion

According to the beam dynamic analysis, the requirement and configuration of each element in the MEBT line have been defined. A copper-plated stainless steel, 3-gap IFMIF-type rebuncher design was selected. The numerical simulations allow us to investigate and optimize the initial rebuncher design.

The first fabricated rebuncher shows a stable and reliable performance during RF power tests (pulsed and CW mode). Our experiments conform in line with our previous studies. The RF conditioning enhances the vacuum level of a factor of three thus reaching a good vacuum level of $2.1 \times 10^{-8} mbar$. The max. temperature of the rebuncher during the power test is much lower than the critical value so that the cooling system performed better than expected. Facing the thermal (cooling water temperature variation and RF loss) induced frequency shift, one side motorized tuner with the closed-loop control system guaranties the rebuncher frequency stability. In addition, the RF power tests

validate the copper-plating technology used by the fabrication company. It is useful to guide the two following rebunchers' fabrication and reduce the risk. Nevertheless, the longitudinal emittance of the beam from the RFQ should be evaluated during the commissioning of the machine to validate all the rebuncher performances.

7. Acknowledgment

We would like to thank DI GIACOMO Marco for useful input and comments regarding preliminary design.

References

[1] A. Kreisel, Saraf phase-i beam operation status, Proc. of LINAC2014, Geneva, Switzerland (2014).

[2] N. Pichoff, D. Berkovits, R. Duperrier, G. Ferrand, B. Gastineau, F. Gougnaud, M. Jacquemet, J. Luner, C. Madec, A. Perry, O. Piquet, T. Plaisant, E. Reinfeld, F. Senée, D. Uriot, The SARAF-LINAC Project 2019 Status, in: 10th International Particle Accelerator Conference, Melbourne, Australia, 2019, p. THPTS116. doi:10.18429/JACoW-IPAC2019-THPTS116. URL https://hal.archives-ouvertes.fr/hal-02283600

[3] D. Berkovits, L. Weissman, A. Arenshtam, Y. B. Aliz, Y. Buzaglo, O. Dudovich, Y. Eisen, I. Eliyahu, G. Feinberg, I. Fishman, et al., Operational experience and future goals of the saraf proton/deuteron linac, Proceedings of LINAC2012, Tel-Aviv, Israel MO1A01 (2012) 100–104.

[4] N. Pichoff, et al., Discussion on SARAF-LINAC Cryomodules, in: 61st ICFA Advanced Beam Dynamics Workshop on High-Intensity and High-Brightness Hadron Beams, 2018, p. TUA2WC01. doi:10.18429/JACoW-HB2018-TUA2WC01.

[5] N. Pichoff, P. Bredy, G. Ferrand, P. Girardot, F. Gougnaud, M. Jacquemet, A. Mosnier, P. Bertrand, M. Di Giacomo, R. Ferdinand, et al., The saraf-linac project for saraf-phase 2, 2015.

[6] D. Uriot, N. Pichoff, Status of tracewin code (2015).

[7] J. Dumas, P. A. P. Nghiem, N. Pichoff, D. Uriot, Beam dynamic studies for the saraf mebt and sc linac (2017).

[8] M. Michel, J.-F. Leyge, D. Uriot, Saraf internal repport: Pdr of saraf-linac major components mebt rebuncher (2015).

[9] J. F. Leyge, M. Michel, Saraf internal report, saraf-00164, Tech. rep., CEA/Ganil (2016).

[10] P. Strehl, Beam Instrumentation and Diagnostics, 2006.

[11] M. Di Giacomo, J. Leyge, M. Michel, P. Toussaint, Design of the mebt rebunchers for the spiral2 driver, LINAC08, Victoria, Canada (2008).

[12] B. Kaizer, J. Rodnizki, E. Farber, A. Perry, L. Danon, Z. Horvitz, O. Mazor, A. Friedman, M. Di Giacomo, J. F. Leyge, M. Michel, P. Toussaint, Study and development of CW room temperature rebuncher for SARAF accelerator, Nuclear Instruments and Methods in Physics Research, Section A: Accelerators, Spectrometers, Detectors and Associated Equipment 871 (2017) 161–168. doi:10.1016/j.nima.2017.04.046.
URL https://linkinghub.elsevier.com/retrieve/pii/S0168900217305211

[13] T. Schilcher, Vector sum control of pulsed accelerating fields in lorentz force detuned superconducting cavities (1998).
URL http://inspirehep.net/record/476909?ln=fr

[14] M. Michel, J. F. Leyge, D. Uriot, Saraf internal report, preliminary design report, Tech. rep., CEA (2016).

[15] F. Gougnaud, Y. Lussignol, F. Gohier, J. F. Denis, T. Joannem, Cea irfu epics environment for the saraf-linac project (2018).

[16] `https://epics.anl.gov/`.

[17] M. Shankar, M. Konrad, L. Li, M. Davidsaver, The epics archiver appliance (2015).